A dynamic wall model for large-eddy simulation of high Reynolds number compressible flows

By S. Kawai AND J. Larsson

1. Motivation and objective

High-speed turbulent boundary-layer flows encompass a range of important phenomena in engineering applications, e.g., aerodynamics and aerothermodynamics of high-speed vehicles. Many of these engineering applications are high Reynolds number flows where small turbulent structures (streaks) near wall region are dynamically important to the separation, reattachment and heat transfer, and thus are critical to the aerodynamics and aerothermodynamics of the vehicle under consideration.

Direct numerical simulation (DNS) and large-eddy simulation (LES) have received increased attention in recent years as powerful tools to study the physics of turbulent boundary layer flows. Their most successful applications, however, have still been for moderate Reynolds numbers, although most engineering applications are at high or very high Reynolds numbers. DNS and LES become prohibitively expensive if one attempts to resolve the small scales (of the order of the viscous scale) of dynamically important turbulent structures near the wall in high Reynolds number flows. Chapman (1979) estimated the number of grid points required for LES of an airfoil to scale as $Re^{1.8}$ when the inner layer is resolved, but only $Re^{0.4}$ when the inner layer is modeled. Thus only Reynolds-averaged Navier-Stokes equations (RANS) or wall-modeled LES (WMLES) can be used to simulate such flows at realistic Reynolds numbers. RANS approaches are presently widely used in engineering practice, but the errors introduced by the turbulence modeling reduce the predictive capability especially for separated non-equilibrium flows.

The WMLES approach generally falls into one of two categories (a review can be found in Piomelli & Balaras 2002): the detached-eddy-simulation (DES, for review, see Spalart 2009) that includes hybrid LES/RANS and the approximate wall-boundary-condition approach (e.g., Deardorff 1970; Schumann 1975; Balaras *et al.* 1996; Cabot & Moin 1999; Wang & Moin 2002). DES is rather popular and is widely used in the compressible flow regime with some success. This approach blends the RANS-type turbulent eddy viscosity $\mu_{t,RANS}$ near the wall with a LES-type subgrid-scale eddy viscosity $\mu_{t,LES}$ away from the wall using a single mesh. Nikitin *et al.* (2000) used the standard DES as a wall model in which the switching location from RANS to LES is placed in the logarithmic region. However, the method is well known to show the logarithmic layer mismatch in the mean velocity profile at the so-called "DES buffer layer," resulting in a predicted skin-friction that is on the order of 15% too low. This could be a critical issue when flow separation, drag or heat transfer are of interest. It was found that in the switching location the eddy-viscosity contribution to mean shear stress is too low, while energy-carrying eddies have not yet been generated (Piomelli *et al.* 2003). Therefore in the DES-type approach, it is necessary to somehow stimulate instabilities and boost the resolved Reynolds stress near RANS and LES interface to improve the logarithmic layer mismatch. Piomelli *et al.* (2003) used the stochastic forcing method and Shur *et al.* (2008) proposed the empirical function of blended length-scale that leads the steep drop of the length scale and the resultant

eddy viscosity to de-stabilize the flow near the interface. Although these adjustments improve the logarithmic layer mismatch, they are to a certain extent empirical rather than physical. For example, when using stochastic forcing, Larsson *et al.* (2006) found that the amplitude of the forcing could be adjusted to give a range of log-layer intercepts. We also note that the recent improvement of DES includes several empirical functions with several parameters (see Shur *et al.* 2008) that make the method more complicated.

The approximate wall-boundary-condition approach is different from the DES-type approach. This approach is based on the solution of a different set of equations in the inner layer (RANS equations) and outer layer (LES equations). The outer-layer LES does not resolve the viscous sublayer, and thus the approximate wall boundary conditions are given by the inner-layer RANS simulation through the wall shear stresses and heat fluxes. Deardorff (1970) and Schumann (1975) introduced the approximate wall boundary conditions by satisfying the logarithmic law in the mean velocity at the first off-wall grid point to model the effect of the wall layer. Balaras *et al.* (1996) and Cabot & Moin (1999) solved the simplified RANS equations, based on the thin boundary-layer approximation, in the wall-layer (inner-layer) on a grid that is refined only in the wall-normal direction to provide the approximate wall boundary condition to the spatially filtered Navier-Stokes (LES) equations in the core of the flow (outer-layer). The wall-layer RANS mesh is embedded in the outer-layer coarse LES mesh (as will be discussed more detail in Section 2.1). Based on the fact that improved solutions were obtained when the mixing-length eddy viscosity was lowered from the standard RANS value (Cabot & Moin 1999), later Wang & Moin (2002) proposed a dynamic procedure to determine the suitable model coefficient for the RANS mixing-length eddy viscosity model. This was then tested at a low Reynolds number ($Re_\theta = 3380$ where wall-resolved LES is accessible) with relatively fine mesh resolution. The grid used in the full wall-resolved LES ($1536\times96\times42$, $\Delta x^+ \approx 62$, $\Delta y^+ \approx 2$, $\Delta z^+ \approx 55$) was coarsened by approximately half in each direction (first grid point at $y^+ \approx 30$) and used for the WMLES mesh ($768\times64\times24$). These approximate wall-boundary-condition approaches have shown reasonable results with smaller log-layer mismatch than is typical in DES. However, these approaches have been mainly investigated in incompressible flows, with little work done for compressible flows. We also note that the dynamic procedure by Wang & Moin (2002) has been tested only on at a single low Reynolds number.

This brief builds on the work of Wang & Moin (2002) and extends it to compressible flows. We also propose a different dynamic procedure that makes the wall model applicable at very high Reynolds number. The proposed wall model is simple and has only one adjustable parameter without the use of *ad hoc* corrections. Mach 1.69 supersonic turbulent boundary layer on a flat plate at $Re_\delta = 61.7 \times 10^4$ ($Re_\theta = 50 \times 10^3$) is simulated. The numerical results are compared with available experimental data (Souverein *et al.* 2010; Souverein 2010).

2. Numerical Framework

2.1. *Wall modeling*

The proposed wall model is based on full compressible RANS calculation in the inner layer. The inner-layer RANS is solved in a grid that is refined in the wall-normal direction and is embedded in the outer-layer coarse LES mesh as illustrated in Figure 1. The LES mesh is designed to resolve the outer-layer scales and does not resolve the viscous sublayer. The RANS calculation is in-time-accurate calculation and provides in-

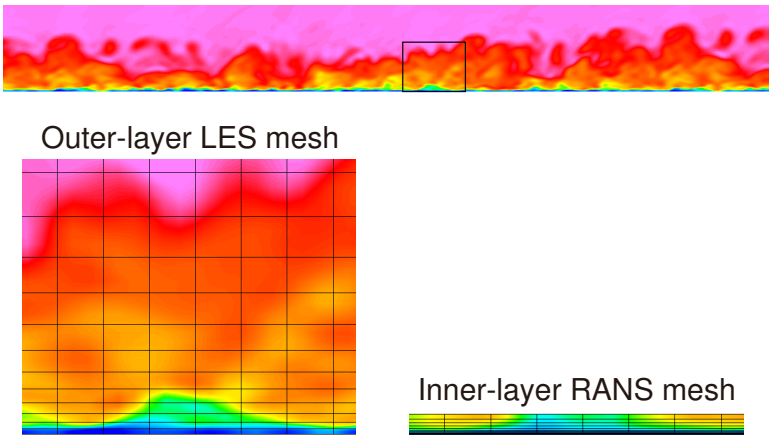

FIGURE 1. Inner-layer RANS and outer-layer LES meshes.

stantaneous wall shear stresses and heat fluxes at wall to the concurrent outer-layer LES as approximate wall boundary conditions. The RANS equations are forced at their top boundary by the instantaneous solution in the LES at the corresponding point. The matching location in the LES mesh where the RANS top boundary matches to the LES mesh is not necessarily at the first off-wall LES nodes (although we note that almost all the previous studies used the first off-wall LES nodes as the matching location) where subgrid modeling and numerical errors are expected to be large mainly due to the poor near-wall resolution in the LES mesh and near boundary scheme (often reduced-order). To allow for the forcing errors due to the subgrid modeling and numerics to be made arbitrarily small, based on our study Larsson & Kawai (2010) fifth grid point off the wall ($y/\delta \approx 0.056$ and $y^+ \approx 860$) in the LES mesh is matched to the RANS top boundary in this study.

2.1.1. *Outer-layer LES*

In the outer layer, compressible spatially-filtered Navier-Stokes equations are solved:

$$\frac{\partial \rho}{\partial t} + \frac{\partial}{\partial x_j}(\rho u_j) = 0, \tag{2.1}$$

$$\frac{\partial}{\partial t}(\rho u_i) + \frac{\partial}{\partial x_j}(\rho u_i u_j) + \frac{\partial p}{\partial x_i} = \frac{\partial \tau_{ij}}{\partial x_j}, \tag{2.2}$$

$$\frac{\partial E}{\partial t} + \frac{\partial}{\partial x_j}[(E+p)u_j] = \frac{\partial}{\partial x_j}(\tau_{ij}u_i) - \frac{\partial q_j}{\partial x_j}, \tag{2.3}$$

$$E = \frac{p}{\gamma - 1} + \frac{1}{2}\rho u_k^2, \quad p = \rho R T, \tag{2.4}$$

where the quantities are spatially-filtered quantities and ρ is the density, u is the velocity, p is the static pressure, E is the total energy, T is the temperature, γ (=1.4) is the ratio of specific heats, and R is the gas constant. The stress tensor τ_{ij} and heat flux vector q_j are

$$\tau_{ij} = 2(\mu+\mu_t)S_{ij} + [\beta - \frac{2}{3}(\mu+\mu_t)]S_{kk}, \quad S_{ij} = \frac{1}{2}\left(\frac{\partial u_i}{\partial x_j} + \frac{\partial u_j}{\partial x_i}\right) \tag{2.5}$$

$$q_j = \frac{1}{\gamma-1}\left(\frac{\mu}{Pr} + \frac{\mu_t}{Pr_t}\right)\frac{\partial c_s^2}{\partial x_j}, \tag{2.6}$$

where μ is the dynamic (shear) viscosity that is computed by Sutherland's law, β is the bulk viscosity ($\beta = 0$ in this study), Pr (=0.72) is the Prandtl number, and c_s is the sound speed. The dynamic Smagorinsky model of Moin *et al.* (1991) with the modification of Lilly (1992) is used to calculate the turbulent eddy viscosity μ_t and turbulent Prandtl number Pr_t.

To solve the LES equations, we impose the wall-normal convective fluxes ρu_j, $\rho u_i u_j$ and $(E+p)u_j$ in Eqs. 2.1–2.3 and the wall-normal viscous flux $\tau_{ij}u_i$ in the energy equation 2.3 to be zero on the wall. Since the LES does not resolve the viscous sublayer, the shear stresses τ_{ij} and heat fluxes q_j at the wall are provided by the concurrent inner-layer RANS simulation. We note that wall-normal derivatives are evaluated using second-order one-sided and central formulae at the first and second grid points off the wall, respectively, while the sixth-order compact differencing scheme (Lele 1992) is used for remaining interior grid points. Given these numerical treatments, therefore, all fluxes in the LES equations can be evaluated without wall boundary conditions since the velocities and temperature at the wall are not well defined in the LES mesh. Although no wall boundary conditions are required for the flux evaluations, we use slip-wall conditions extrapolated from the interior nodes to calculate the dynamic Smagorinsky model and apply a low-pass spatial filtering.

2.1.2. *Inner-layer RANS*

The full compressible RANS equations are solved on an embedded near-wall mesh to provide wall shear stresses and heat fluxes to the outer-layer LES. The time-accurate inner-layer flow is calculated with no-slip adiabatic wall conditions, and the primitive quantities (ρ, u_i and p) at the top boundary are forced by the instantaneous outer-layer LES calculation at the corresponding points.

In addition to solving the full RANS equations, we also consider the equilibrium-boundary-layer equations:

$$\frac{d}{dy}\left[(\mu+\mu_t)\frac{du}{dy}\right] = 0 \tag{2.7}$$

$$\frac{d}{dy}\left[(\mu+\mu_t)\,u\frac{du}{dy} + \frac{1}{\gamma-1}\left(\frac{\mu}{Pr} + \frac{\mu_t}{Pr_t}\right)\frac{dc_s^2}{dy}\right] = 0. \tag{2.8}$$

Since these simple equations are supposed to be accurate for zero-pressure-gradient equilibrium flows considered in this study, we can compare this simple model with the full RANS model to investigate the capability of the full RANS model. In this simple model, the pressure is assumed to be wall-normal independent and equal to the outer-layer LES solution at the RANS top boundary while the full RANS equations solve the pressure. We note that these simple equations are ordinary differential equations (ODE) and easy to implement.

The simple mixing-length eddy-viscosity model with near-wall damping is used to determine the μ_t in the inner-layer RANS as

$$\mu_t = \kappa\rho y\sqrt{\frac{\tau_w}{\rho}}\mathcal{D}, \quad \mathcal{D} = \left[1-\exp(-y^+/A)\right]^2, \tag{2.9}$$

where $A = 17$, y^+ is the distance from the wall in wall units, and ρ and τ_w are the local instantaneous density and wall stress. The turbulent Prandtl number Pr_t is fixed to 0.9 when the dynamic procedure discussed in the following section 2.1.3 is not used.

2.1.3. *Dynamic procedure*

To close the system of equations, one must set the two undefined parameters κ in Eq. 2.9 and Pr_t in the inner-layer RANS equations. Wang & Moin (2002) introduced a dynamic procedure to adjust the model coefficient κ. The idea of Wang & Moin (when extended to compressible flow) is to match the total shear stress $-\overline{\rho}\widetilde{u''v''}+(\overline{\mu}+\overline{\mu_t})\partial\widetilde{u}/\partial y$ between the LES and RANS at the matching location. Since the velocity, density and temperature are given from the LES as a boundary condition for RANS, this means that the resolved portion is identical in LES and RANS at the matching location. If one further assumes that the velocity and temperature have the same slope in RANS and LES, the matching condition amounts to matching $\mu_{t,LES}$ and $\mu_{t,RANS}$. Wang & Moin (2002) matched the eddy-viscosities $\langle\mu_{t,RANS}\rangle = \langle\mu_{t,LES}\rangle$ (where $\langle\cdot\rangle$ was taken as the average in the spanwise direction and over the previous 150 time steps), and thus approximately matched the total shear stresses. The resultant reduced κ was then applied throughout the boundary layer in the RANS. This dynamic procedure was tested through the incompressible turbulent boundary layer flow past an airfoil trailing-edge at low Reynolds number ($Re_\theta = 3380$ where wall-resolved LES data are available), and they found that improved results were obtained by the dynamic procedure compared with a constant coefficient (κ=0.41). Note that since they used an incompressible flow solver, there was no need to define the turbulent Prandtl number.

In the present study, we propose a simple mesh-resolution-dependent dynamic procedure for compressible flows where the heat fluxes are present in addition to the shear stresses. Since the velocities and temperature are matched at the top of the inner-layer RANS, the resolved portion of the stresses and heat fluxes from the inner- and outer-layer calculations are the same. To match the total stresses and heat fluxes approximately at the matching location, the unresolved stresses and heat fluxes need to be matched. Similarly to the procedure of Wang & Moin (2002), we dynamically adjust the κ and Pr_t in the inner-layer RANS equations by imposing $\langle\mu_{t,RANS}\rangle = \langle\mu_{t,LES}\rangle$ (that is, $\hat{\kappa} = \langle\mu_{t,LES}\rangle/\langle\rho y\sqrt{\frac{\tau_w}{\rho}}\mathcal{D}\rangle$) and $\hat{\mathrm{Pr}}_{t,RANS} = \langle\mathrm{Pr}_{t,LES}\rangle$ at the matching location to approximately match the unresolved components. Here the dynamically computed $\hat{\kappa}$ and $\hat{Pr}_t$ are functions of the streamwise location. We note that here the averaging denoted by the angular brackets is performed in the homogeneous direction (spanwise direction in the present study).

The objective of the mesh-resolution-dependent (wall-normal-dependent) dynamic procedure is to approximately account for the fact that the division between resolved and unresolved stresses changes dramatically in the wall-normal direction in the near-wall RANS, partly due to the exceedingly anisotropic mesh used at high Reynolds number for the RANS. The length scale in the wall-parallel direction $\lambda_\parallel$ of the energetic and stress-carrying motions in the log-layer is proportional to the the distance from wall. Thus one can assume the length scale of the stress-carrying motions as $\lambda_\parallel = C_L y$, where $C_L \approx 2.5$ (Pope 2000) and y is the wall-normal distance. If the ratio of the length scale

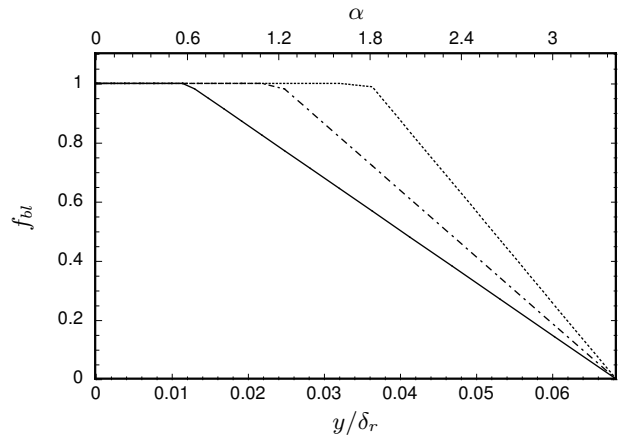

FIGURE 2. Linear blending function f_{bl}. Solid line, $\alpha = 0.6$; dashed-dotted line, $\alpha = 1.2$; dotted line, $\alpha = 1.8$.

to the wall-parallel grid spacing $\lambda_\parallel/\Delta_\parallel$ is smaller than some constant α, we may assume that the resolved stress is negligibly small. Thus typical RANS constants, $\kappa = 0.41$ and $Pr_t = 0.9$, should be used. If $\lambda_\parallel/\Delta_\parallel > \alpha$, the constants should be blended with the adjusted constants toward the matching location. We note that the length scale of the stress-carrying motions in the wall-normal direction λ_y is certainly smaller than $\lambda_\parallel$. Since the RANS mesh is significantly refined in the wall-normal direction to resolve the viscous layer in the RANS sense, Δy is fine enough to resolve λ_y and also $\Delta y < \Delta_\parallel$. In this study, we use the linear blending as

$$\kappa = 0.41 f_{bl} + \hat{\kappa}(1 - f_{bl}) \tag{2.10}$$

$$Pr_t = 0.9 f_{bl} + \hat{Pr}_t(1 - f_{bl}), \tag{2.11}$$

where

$$f_{bl} = \begin{cases} 1 & \lambda_\parallel/\Delta_\parallel \le \alpha \\ \frac{\lambda_{\parallel,top}/\Delta_\parallel - \lambda_\parallel/\Delta_\parallel}{\lambda_{\parallel,top}/\Delta_\parallel - \alpha} & \lambda_\parallel/\Delta_\parallel > \alpha. \end{cases} \tag{2.12}$$

$\lambda_{\parallel,top}$ is the approximate length-scale at the matching location (top boundary), $\lambda_{\parallel,top} = C_L y_{top}$. Figure 2 shows the linear blending function f_{bl} with different constant α. In this study, we define the wall-parallel grid spacing as $\Delta_\parallel = \max(\Delta_x, \Delta_z)$. The scale of $\Delta_\parallel$ can be considered as approximately equivalent to the smallest eddy size that the mesh can possibly support if an isotropic eddy is considered. Also, we note that in practice the grid for the outer-layer LES may be nearly isotropic, and thus the impact of this specific choice is not considered to be crucial. The only adjustable parameter in the model is α, and in Section 3.2 we address the sensitivity of flow statistics to α.

In this study, we compare the dynamic procedure proposed above with the wall-normal independent dynamic-coefficient approach ($\kappa = \hat{\kappa}$ and $Pr_t = \hat{Pr}_{t,RANS}$, essentially the choice of Wang & Moin 2002). The present study also revisits the constant-coefficient approach ($\kappa = 0.41$ and $Pr_t = 0.9$) and equilibrium-boundary-layer approach (solving ODEs of 2.7 and 2.8) and compares the constant-coefficient models with the dynamic models.

2.2. *Numerical scheme*

The spatial derivatives for interior nodes in both the inner-layer RANS and outer-layer LES equations are evaluated by the sixth-order compact differencing scheme (Lele 1992). At boundary points 1, 2 and 3 and correspondingly at $imax$, $imax$-1 and $imax$-2 in the outer-layer LES, second-order one-sided and second-order central formulas are utilized. In the inner-layer RANS, the second- and fourth-order one-sided formulae are used for the first and second grid point near the boundary. An eighth-order low-pass spatial filtering scheme (Lele 1992; Gaitonde & Visbal 2000) with $\alpha_f = 0.495$ is applied to the conservative variables. The classical, four-stage, fourth-order, low-storage form of the Runge-Kutta method is used for time integration in the outer-layer LES. To alleviate a severe Courant-Friedrichs-Lewy time-step restriction in the inner-layer RANS computation due to the highly refined mesh in wall-normal direction, the second-order fully implicit time-integration scheme (Obayashi *et al.* 1988; Iizuka 2006) is used in the inner-layer RANS computation. Three steps of sub-iterations (Newton-Raphson iteration) are adopted to minimize the errors due to the linearization in the implicit scheme.

2.3. *Computational grids*

The computational domain size for the WMLES is $15\delta_r$, $15\delta_r$ and $3\delta_r$ in streamwise (x), wall-normal (y) and spanwise (z) directions where δ_r is the reference boundary layer thickness that is close to the boundary thickness at the inlet. The boundary layer thickness δ at the station where statistics are compared is $\delta \approx 1.2\delta_r$. A buffer layer with the length of $12\delta_r$ is placed at the upper boundaries to remove turbulent fluctuations and their reflection from the boundary. A uniformly spaced grid, $\Delta x/\delta_r = 0.05$ and $\Delta z/\delta_r = 0.03$, is adopted in the streamwise and spanwise directions. In the wall-normal direction, the grid is smoothly stretched in the region y/δ_r=0 to 1.4 and then a uniformly spaced grid is used from y/δ_r=1.4 to 3. The grid resolutions at the wall and uniformly spaced region are $\Delta y/\delta_r = 0.0125$ and $\Delta y/\delta_r = 0.04$, respectively. In viscous wall units, these grid resolutions are $\Delta x^+ \approx 613$, $\Delta y^+ \approx 153$ to 490 and $\Delta z^+ \approx 368$. The horizontal (wall-parallel plane) mesh distributions for the inner-layer RANS mesh are the same as the outer-layer LES mesh while the RANS mesh is significantly refined in the wall-normal direction (y^+ at the first grid point off the wall is less than 1) to resolve the viscous sublayer. We note that no complex procedure is necessary to generate the inner-layer RANS mesh since only the wall-normal refinement is required, which can be easily done within the preprocess of simulation. The rescaling-reintroducing method of Urbin & Knight (2001) is used to generate the inflow conditions for both the inner-layer RANS and outer-layer LES. The flow quantities at the $12\delta_r$ downstream location are rescaled and reintroduced for the inflow conditions.

3. Results

The flow condition considered in this study is based on the experiments of high Reynolds number supersonic turbulent boundary layer on a flat plate performed by Souverein *et al.* (Souverein *et al.* 2010; Souverein 2010). The freestream Mach number is 1.69 and the Reynolds number is $Re_\delta = 61.7 \times 10^4$ ($Re_\theta = 50.0 \times 10^3$). Four different inner-layer RANS models are considered while the outer-layer LES simulation is the same:

1. EQBL: equilibrium boundary layer approach (solving ODEs of 2.7 and 2.8),
2. CNST: full RANS + constant coefficients (κ=0.41 and Pr_t=0.9),

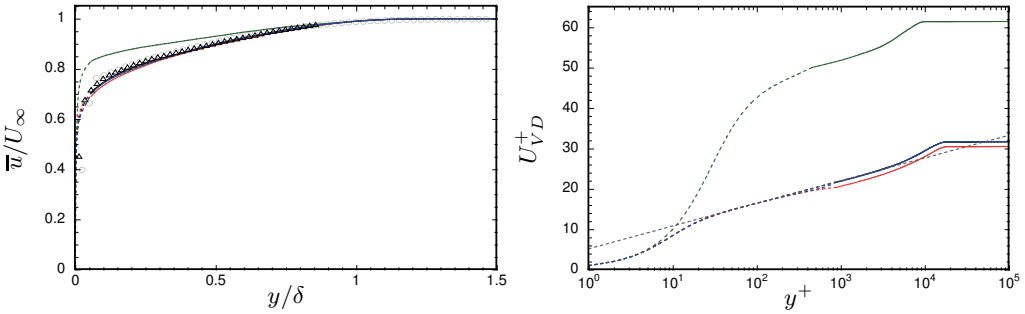

FIGURE 3. Mean streamwise velocity profiles: δ scaling on left and Van Driest scaling on right. EQBL (black), CNST (red, lowest curve), CDYN (green, uppermost curve), VDYN with $\alpha = 1.2$ (blue), Log-law $U^+_{VD} = 1/0.41\log(y^+) + 5.2$ (dashed). Symbols (circles, dual-PIV; triangles, high-resolution zoom-PIV), experiments by (Souverein 2010). Solid lines, outer-layer WMLES; dashed lines, inner-layer RANS.

3. CDYN: full RANS + y-constant dynamic approach ($\kappa = \hat{\kappa}$ and $Pr_t = \hat{P}r_{t,RANS}$),
4. VDYN: full RANS + y-variable dynamic approach (Eqs. 2.10 and 2.11).

3.1. *Comparison with dynamic models and constant-coefficient models*

Figure 3 shows the mean streamwise velocity profiles where the results of the outer-layer wall-modeled LES and inner-layer RANS are plotted with solid and dashed lines, respectively. As expected, EQBL in the inner-layer RANS is in excellent agreement with the log law, showing the validity of the equilibrium-boundary-layer equations for zero-pressure-gradient attached flows. The VDYN result is almost identical to the EQBL result and in good agreement with the experiments and the log law. The logarithmic region appears clearly in the range of $30 < y^+ < 3000$ without showing the logarithmic layer mismatch. Although the slope of the logarithmic region is well predicted in CNST, the CNST result shows a lower intercept, indicating higher skin friction (8.7% higher than EQBL). This trend is consistent with the finding of Wang & Moin (2002). As pointed out by Cabot & Moin (1999), since the Reynolds stress carried by the nonlinear convective terms in the RANS equations is significant near the matching location, RANS eddy viscosity model must be reduced to account for only the unresolved components. CDYN is the wall-normal-independent dynamic-coefficient approach and essentially the choice of Wang & Moin (2002). This model approximately matches the total stress at the matching location and assumes the wall-normal-independent coefficient ($\kappa = \hat{\kappa}$ and $Pr_t = \hat{P}r_{t,RANS}$). Although the total stress is approximately matched at the RANS top boundary, y-constant dynamic procedure reduces the value of κ with a constant factor ($\approx 1/50$ at this high Reynolds number flow) throughout the inner-layer and laminarizes the inner-layer flow, resulting in the intercept too high (low skin friction) for this high Reynolds number flow.

This is also evident in the mean turbulent eddy viscosity profiles for the four different inner-layer RANS models as shown in Figure 4. The CDYN approach reduces the turbulent eddy viscosity significantly throughout the boundary layer, and $\mu_t/\mu \approx 10$ at the matching location. On the other hand, the VDYN approach maintains the original RANS eddy viscosity up to $\lambda_\parallel/\Delta_\parallel = 1.2$ location as designed and gradually reduces μ_t toward the matching location where the total stress between inner and outer layer is approximately matched. The results indicate that the unresolved stresses and heat fluxes are increased in the wall-normal direction from the matching location toward the wall

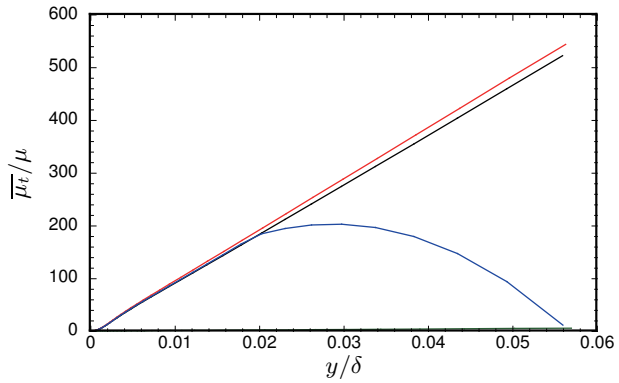

FIGURE 4. Mean turbulent eddy viscosity in inner-layer RANS. EQBL (black), CNST (red, uppermost curve), CDYN (green, close to horizontal axis), VDYN with $\alpha = 1.2$ (blue, curved shape).

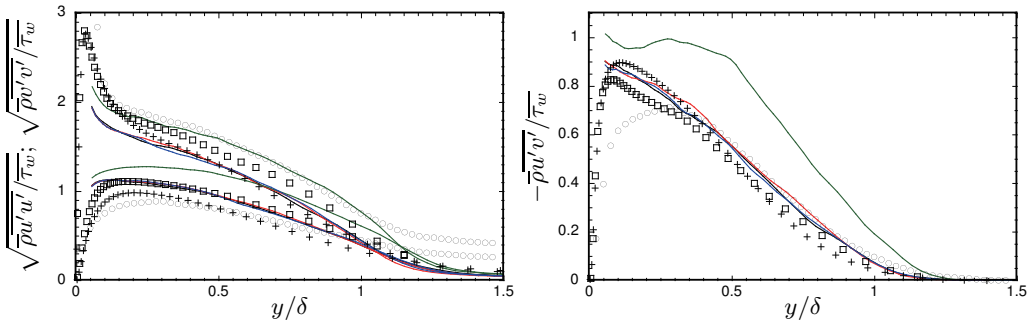

FIGURE 5. Resolved velocity fluctuations (left: upper curves, u'; lower curves, v') and Reynolds shear stress (right) for outer-layer WMLES. Black, EQBL; red line, CNST; green, CDYN; blue, VDYN ($\alpha = 1.2$); circles (dual-PIV), experiments (Souverein 2010); squares, DNS at Mach 2.28 and $Re_\theta \approx 2300$ (Pirozzoli & Bernardini 2010); pluses, incompressible DNS at $Re_\theta = 900$ (Wu & Moin 2009).

in the RANS mesh and this physics must be properly modeled. The proposed y-variable dynamic approach (VDYN) that approximately accounts for this physics is shown to be superior to the other models. The successful results obtained by the y-constant dynamic procedure by Wang & Moin (2002) for their case is probably due to the fact that their flow condition is at the moderate Reynolds number ($Re_\theta = 3380$). In fact, they reported that in their calculation the factor of y-constant reduction of κ is approximately 1/5 (where as a factor of 1/50 is found for the much higher Reynolds number in the present study).

Resolved velocity fluctuations and Reynolds shear stress for outer-layer WMLES are plotted in Figure 5 with the experimental data (Souverein 2010) and compressible and incompressible DNS data at low Reynolds numbers (Pirozzoli & Bernardini 2010; Wu & Moin 2009). EQBL, CNST and VDYN show almost identical results and reasonable agreement with the experimental data and DNS data. Only the CDYN results behave differently. This is primarily because of the too-low wall shear stress (approximately 1/4 of EQBL) given by the CDYN model, resulting in the lower velocity fluctuations and Reynolds shear stress. Note that the τ_w normalization used in Figure 5 causes the

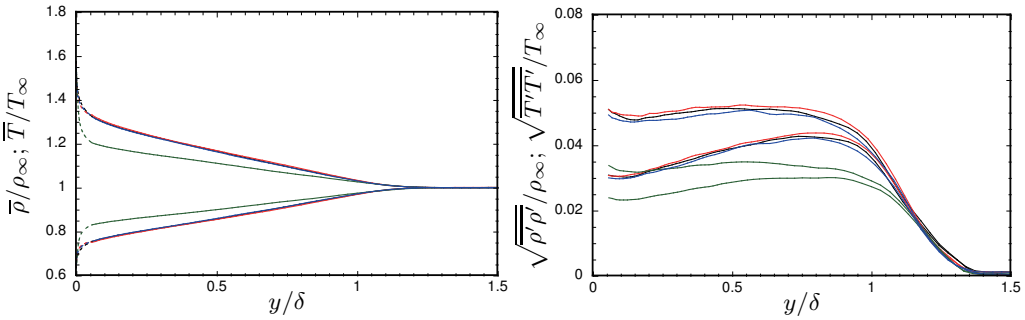

FIGURE 6. Mean and fluctuation density (lower curves) and temperature (upper curves) for outer-layer WMLES. Black, EQBL; red line, CNST; green, CDYN; blue, VDYN ($\alpha = 1.2$).

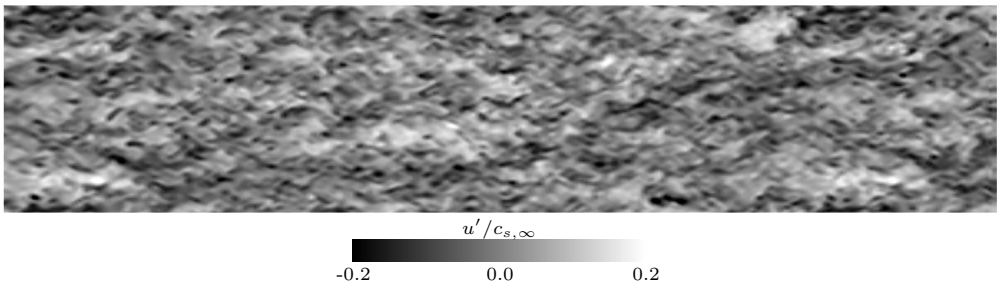

FIGURE 7. Instantaneous streamwise velocity fluctuation in a wall-parallel plane at the matching location ($y/\delta = 0.056$, $y^+ = 856$). The figure covers the full domain, i.e., 15×3 in terms of the boundary layer thickness at the inlet.

higher values of CDYN, although the actual fluctuations obtained by CDYN are smaller than the others. As noted in Souverein (2010), the experimental velocity fluctuations include a contribution from the measurement noise, and the noise likely causes the slight overestimation of the u-fluctuations compared to the DNS data. The underestimation of the v-fluctuations is a measurement artifact, related to the dynamic range of the measurement system and the measurement settings. By consequence, the under-resolved v-fluctuations lead to underestimated Reynolds shear stress values, particularly below $y/\delta = 0.3$. Figure 6 shows mean and fluctuation density and temperature profiles. EQBL, CNST and VDYN again show almost identical results, whereas the CDYN results show less thermodynamic fluctuations and resultant less turbulent mixing.

Figure 7 shows contours of the instantaneous streamwise velocity fluctuations in wall-parallel plane at the matching location (logarithmic region: $y/\delta = 0.056$, $y^+ = 856$) obtained by the WMLES with the y-variable dynamic approach (VDYN). The present WMLES does not produce smooth nearly one-dimensional unphysical eddies without the use of *ad hoc* corrections, while the standard DES wall-layer model suffers from the unphysical structures (Piomelli & Balaras 2002).

3.2. *Sensitivity to α in the y-variable dynamic approach*

The only adjustable parameter in the y-variable dynamic approach is α. The α indicates the location where the original RANS eddy viscosity and turbulent Prandtl number start blending with the adjusted constants. Therefore if the result is too sensitive to α, the

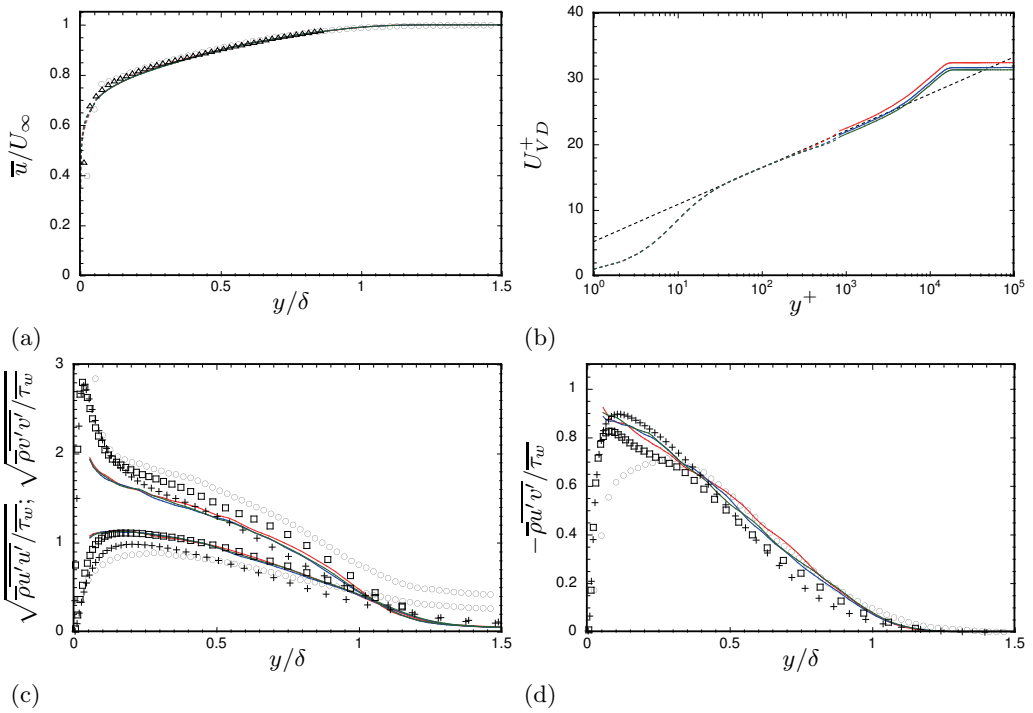

FIGURE 8. Sensitivity of statistics to α in the y-variable dynamic approach: (a) mean velocity in δ scaling, (b) mean velocity in Van Driest scaling, (c) variances of streamwise (upper curves) and wall-normal velocity (lower curves), (d) Reynolds shear stress. Red, $\alpha = 0.6$; blue, $\alpha = 1.2$; green, $\alpha = 1.8$; gray dashed line, $U^+_{VD} = 1/0.41\log(y^+) + 5.2$; circles (dual-PIV) and triangles (high-resolution zoom-PIV), experiments (Souverein 2010); squares, DNS at Mach 2.28 and $Re_\theta \approx 2300$ (Pirozzoli & Bernardini 2010); pluses, incompressible DNS at $Re_\theta = 900$ (Wu & Moin 2009). Solid lines, outer-layer WMLES; dashed lines, inner-layer RANS.

applicability of the model might be reduced. Here we address this issue by investigating the sensitivity of flow statistics to α.

The sensitivity of the flow statistics to α in the y-variable dynamic approach is shown in Figure 8. The choices of $\alpha = 0.6$, 1.2 and 1.8 start blending the eddy viscosity and turbulent Prandtl number at $y/y_{top} = 0.19$, 0.36 and 0.53 (see Figure 2) respectively, where y_{top} is the wall-normal distance at the RANS top boundary. All the results agree reasonably well with the experimental data and DNS data. It was found that the results are largely insensitive to the choice of α, and with the current numerical schemes the choice of $\alpha = 1.2$ was found to yield the best results. The wall shear stress is slightly underestimated by 3.5% with $\alpha = 0.6$ and overestimated by 3.2% with $\alpha = 1.8$ when compared with the EQBL result. Although not shown here, thermodynamic quantities are also insensitive to α. As discussed in Section 2.1.3, since the scale of $\Delta_\parallel$ can be considered as approximately the smallest eddy size that the mesh can possibly support when assuming an isotropic eddy, the best results obtained by $\alpha = 1.2$ seem reasonable.

4. Conclusions and future work

We proposed a simple mesh-resolution-dependent (y-variable) dynamic wall model for LES of compressible flows and applied to the supersonic turbulent boundary layer on a

flat plate at $Re_\theta = 50 \times 10^3$. The wall model approximately matches the total stresses and heat fluxes at the matching location and also accounts for the physics that the unresolved stresses and heat fluxes are increased in the wall-normal direction toward the wall in the inner-layer RANS. This dynamic concept may be applicable to both incompressible and compressible flows, although we only applied it to the compressible flow. The model has only one adjustable parameter α, but the value of α considered in this study did not affect the results significantly, showing the robustness of the model. The proposed y-variable dynamic wall model showed successful agreements with the available experimental data without showing the typical logarithmic layer mismatch. Also, the WMLES does not produce large unphysical eddies without *ad hoc* corrections. Neither the constant nor the y-independent dynamic coefficient model were able to predict the correct intercept in the Van Driest transformed velocity, although the slope of the logarithmic region is reasonable. The LES with constant coefficient model showed a low intercept, indicating high skin friction by 8.7%. The wall-normal independent (y-constant) dynamic model excessively reduces the turbulent eddy viscosity throughout the inner-layer RANS region and laminarizes the flow, resulting in the intercept too high (low skin friction) for this high Reynolds number flow.

Further detailed investigations of the model at moderate Reynolds number, mesh resolution sensitivity and the impact of numerical errors near wall-region in the outer-layer LES are the focus of ongoing research and will be discussed in Kawai & Larsson (2011). Future work will also include the application of the wall model to non-equilibrium shock wave and turbulent boundary layer interaction flows.

Acknowledgments

This work is supported by National Aeronautics and Space Administration Hypersonics Project. Computer time was provided by High Performance Computing Center at Stanford University. The authors gratefully acknowledge Louis J. Souverein for providing extensive experimental data, and Sergio Pirozzoli and Xiaohua Wu for providing DNS data used for comparison here. We are grateful to Sanjiva K. Lele for valuable discussions. The present code is based on an extension to the code FDL3DI provided by Miguel R. Visbal at the Air Force Research Laboratory, whom the authors also would like to thank.

REFERENCES

Balaras, E., Benocci, C. & Piomelli, U. 1996 Two-layer approximate boundary conditions for large-eddy simulations. *AIAA J.* **34** (6), 1111–1119.

Cabot, W. & Moin, P. 1999 Approximate wall boundary conditions in the large-eddy simulation of high Reynolds number flow. *Flow Turbul. Combust.* **63** (1–4), 269–291.

Chapman, D. R. 1979 Computational aerodynamics development and outlook. *AIAA J.* **17** (12), 1293–1313.

Deardorff, J. W. 1970 A numerical study of three-dimensional turbulent channel flow at large Reynolds number. *J. Fluid Mech.* **41**, 453–480.

Gaitonde, D. V. & Visbal, M. R. 2000 Padé-type higher-order boundary filters for the Navier-Stokes equations. *AIAA J.* **38** (11), 2103–2112.

Iizuka, N. 2006 Study of mach number effect on the dynamic stability of a blunt re-entry capsule. PhD thesis, University of Tokyo.

Kawai, S. & Larsson, J. 2011 Wall modeling in large-eddy simulation: predicting accurate skin friction at very high Reynolds number. In *Proceeding of 49th AIAA Aerospace Sciences Meeting*. AIAA.

Larsson, J., Lien, F. S. & Yee, E. 2006 Feedback-controlled forcing in hybrid LES/RANS. *Int. J. CFD* **20** (10), 687–699.

Larsson, J. & Kawai, S. 2010 Wall-modeling in large eddy simulation: length scales, grid resolution and accuracy. In *Annual Research Briefs*. Center for Turbulence Research, Stanford University.

Lele, S. K. 1992 Compact finite difference schemes with spectral-like resolution. *J. Comput. Phys.* **103** (1), 16–42.

Lilly, D. K. 1992 A proposed modification of the Germano subgrid-scale closure method. *Phys. Fluids A* **4** (3), 633–635.

Moin, P., Squires, K., Cabot, W. & Lee, S. 1991 A dynamic subgrid-scale model for compressible turbulence and scalar transport. *Phys. Fluids A* **3** (11), 2746–2757.

Nikitin, N. V., Nicoud, F., Wasistho, B., Squires, K. D. & Spalart, P. R. 2000 An approach to wall modeling in large-eddy simulations. *Phys. Fluids* **12** (7), 1629–1632.

Obayashi, S., Fujii, K. & Gavali, S. 1988 Navier-Stokes simulation of wind-tunnel flow using LU-ADI factorization algorithm. NASA-TM-100042. NASA.

Piomelli, U. & Balaras, E. 2002 Wall-layer models for large-eddy simulations. *Annu. Rev. Fluid Mech.* **34**, 349–374.

Piomelli, U., Balaras, E., Pasinato, H., Squires, K. D. & Spalart, P. R. 2003 The inner-outer layer interface in large-eddy simulations with wall-layer models. *Intl J. Heat Fluid Flow* **24** (4), 538–550.

Pirozzoli, S. & Bernardini, M. 2010 A DNS database for impinging shock/turbulent boundary layer interaction. *AIAA J.* submitted.

Pope, S. B. 2000 *Turbulent Flows*. Cambridge University Press.

Schumann, U. 1975 Subgrid scale model for finite difference simulations of turbulent flows in plane channels and annuli. *J. Comput. Phys.* **18** (4), 376–404.

Shur, M. L., Spalart, P. R., Strelets, M. K. & Travin, A. K. 2008 A hybrid RANS-LES approach with delayed-DES and wall-modelled LES capabilities. *Intl J. Heat Fluid Flow* **29** (6), 1638–1649.

Souverein, L. J. 2010 On the scaling and unsteadiness of shock induced separation. PhD thesis, Delft University of Technology.

Souverein, L. J., Dupont, P., Debieve, J. F., Dussauge, J. P., van Oudheusden, B. W. & Scarano, F. 2010 Effect of interaction strength on unsteadiness in turbulent shock-wave-induced separations. *AIAA J.* **48** (7), 1480–1493.

Spalart, P. R. 2009 Detached-eddy simulation. *Annu. Rev. Fluid Mech.* **41**, 181–202.

Urbin, G. & Knight, D. 2001 Large-eddy simulation of a supersonic boundary layer using an unstructured grid. *AIAA J.* **39** (7), 1288–1295.

Wang, M. & Moin, P. 2002 Dynamic wall modeling for large-eddy simulation of complex turbulent flows. *Phys. Fluids* **14** (7), 2043–2051.

Wu, X. & Moin, P. 2009 Direct numerical simulation of turbulence in a nominally zero-pressure-gradient flat-plate boundary layer. *J. Fluid Mech.* **630**, 5–41.